Modeling of novel heterojunction tunnel structures

D. Z.-Y. Ting, E. T. Yu, D. A. Collins, D. H. Chow, and T. C. McGill
Thomas J. Watson, Sr. Laboratory of Applied Physics, California Institute of Technology, Pasadena, California 91125

(Received 31 January 1990; accepted 10 April 1990)

We have implemented a simple model that allows realistic yet rapid simulation of conventional as well as interband resonant tunneling devices. Using this model we have studied GaAs/AlAs asymmetric triple barrier structures and found that coherence between the quasibound states in the two quantum wells should be observable in the I–V characteristics of the devices. We have also examined InAs–GaSb–InAs broken-gap interband tunnel devices and found that, despite the absence of classically forbidden barrier regions, a resonant tunneling process is involved in producing the observed negative differential resistance. Furthermore, we have found that maximum peak current densities should be found in devices with GaSb layer thicknesses corresponding to a single, rather than a multiple transmission resonance peak in the broken-gap region.

I. INTRODUCTION

Since the original proposal[1] and observation[2] of negative differential resistance (NDR) in heterojunction resonant tunneling devices, the subject has undergone intense theoretical and experimental investigation. Perhaps the most common platform for realizing NDR is the double barrier heterostructure (DBH) device, in which conduction band electrons undergo resonant tunneling through quasibound conduction band states.

Recently, NDR has been proposed and experimentally observed in a new class of tunnel structures made from InAs, GaSb, and AlSb.[3-8] These so-called interband tunnel devices differ from the conventional resonant tunneling devices in that the tunneling processes involve both the conduction and valence bands. The first such device utilized tunneling of conduction band electrons through valence band quasibound states;[4] subsequently, devices involving holes tunneling through conduction band quasibound states,[5,6] and conduction band electrons tunneling into valence band states[5] have also been demonstrated. In addition to their novel tunneling mechanisms, which are of scientific interest, interband tunnel devices have also been shown to exhibit interesting electrical properties which may have practical consequences. For example, a peak-to-valley current ratio of 20 (88) at 300 K (77 K) has been reported in an InAs–AlSb–GaSb–AlSb–InAs device,[4] and NDR with a peak current density of 2.4×10^4 A/cm^2 has been observed in an InAs–GaSb–InAs device.[8]

In this paper we present a model suitable for studying both conventional and interband resonant tunneling devices. The model was formulated with the following requirements in mind: (1) Both the electron and hole bands must be considered in order to account for the interband tunneling processes. (2) Realistic band bending must be included so that the effects of various doping schemes on device performance can be evaluated. (3) The model must be numerically efficient so that simulation can be completed in a relatively short time period. This is especially useful in designing new devices in which a large parameter space (e.g., material sequence, layer thicknesses, and doping profile) must be explored quickly.

Using these criteria, we have developed a method for computing J-V characteristics of heterostructure devices based on a simple two-band model. The method is described in Sec. II. Applications of the method are demonstrated in Sec. III where we (a) illustrate how wave function engineering might be used to improve device performance in GaAs/AlAs asymmetric triple barrier resonant tunnel structures, and (b) analyze the interband resonant tunneling process in InAs–GaSb–InAs heterostructures.

II. THEORETICAL MODEL

Our computation of current-voltage (J-V) characteristics can be divided into three steps. First, band bending corresponding to the given doping profile and applied bias is computed. Transmission coefficients are then calculated using a transfer matrix technique[9] for a two-band model, described below. Finally, current is computed by including appropriate Fermi factors and velocities, and integrating over the incoming electron distribution. Our calculation stays within the framework of the single-electron picture, and does not include effects due to inelastic scattering. Because inelastic tunneling processes are neglected, we have not attempted to estimate the valley current in the devices that we model.

For a given doping profile and applied bias, band bending is computed by solving Poisson's equation across the entire device and requiring overall charge-neutrality in the structure. Thomas–Fermi screening theory is used to relate the local carrier concentration to the band-edge position.

Given the band diagram, the transmission coefficient as a function of incoming electron energy $T(E)$ is computed using a transfer matrix technique. The band structure is described by a simple two-band local orbital model in which only the lowest conduction band and the light hole band are included. In this model, we consider a linear chain occupied by alternating s and p orbitals. The on-site energies of the s and p orbitals are E_s and E_p, respectively, and the nearest neighbor interaction between s and p orbitals is taken to be

 0734-211X/90/040810-07$01.00 © 1990 American Vacuum Society

$+t$ or $-t$, depending on whether the s orbital is closer to the positive or to the negative lobe of the p orbital. A diagram of the orbitals and nearest-neighbor interactions is shown in Fig. 1(a). E_s and E_p are the conduction and valence band edges, respectively, and t is determined from the effective mass (m^*):

$$t^2 = \frac{\hbar^2}{2m^*d^2}(E_s - E_p), \tag{1}$$

where d is the distance between successive unit cells. The bulk band structure for this model, shown schematically in Fig. 1(b), is given by

$$(E - E_s)(E - E_p) = 4t^2 \sin^2(kd/2), \tag{2}$$

which is similar to that given by Kane's two-band model:

$$(E - E_c)(E - E_v) = (\hbar \mathbf{k}\cdot\mathbf{p}/m)^2. \tag{3}$$

Note that in both of these models, the electron and light hole effective masses are identical. This is a reasonable approximation for the materials discussed in this paper (e.g., for InAs, $m_e = 0.023m_0$, $m_{lh} = 0.025m_0$).

Once we have bulk material parameters E_s, E_p, and t, we can construct the heterostructure Hamiltonian from the parameters for the constituent materials. At a heterojunction, the hopping matrix element t is taken to be the arithmetic mean of those for the two materials forming the junction. A transfer matrix technique is then applied to compute the transmission coefficient. We found that in practice, the *sp* two-band model is faster than previous calculations[10] using Kane's two-band model by approximately an order of magnitude.

A major drawback of this simple model is the omission of the heavy hole bands which can have substantial interaction with the light hole band in heterostructures.[11] Heavy hole–light hole mixing and spin–orbit interaction could be important for the analyses of some of the interband devices, and these effects are currently being investigated. Because of its simplicity, however, the *sp* two-band model does have some practical advantages, including (1) computational efficiency, and (2) numerical stability in transfer matrix computations due to the lack of complex bands with large imaginary k vectors (corresponding to rapidly growing and decaying states) in the energy range of interest.

Once the transmission coefficient $T(E)$ is computed, the current can be computed using the standard formula:[12]

$$j = \frac{e}{4\pi^3\hbar}\int d^2k_{\parallel}\int dE\,[f(E) - f(E+eV)]\,T(E,k_{\parallel}). \tag{4}$$

III. RESULTS AND DISCUSSION

To illustrate the use of our model, we have analyzed two types of structures. In the first case, we study GaAs/AlAs asymmetric triple barrier heterostructures, and in the second we examine InAs–GaSb–InAs interband tunnel devices.

A. Asymmetric triple barriers

For our first example, we examine GaAs/AlAs asymmetric triple barrier heterostructures. As pictured in Fig. 2, the triple barrier structure consists of three AlAs barrier layers, labeled B1, B2, and B3, embedded in GaAs, and thereby forming two quantum GaAs wells labeled W1 and W2. For our purposes we let the widths of B1 and B3 (L_{B1} and L_{B3}), be the same, and we let B2 be sufficiently narrow to allow for the possibility of strong mixing of the quasibound states in W1 and W2. The asymmetry refers to the fact that the well widths L_{W1} and L_{W2} are different.

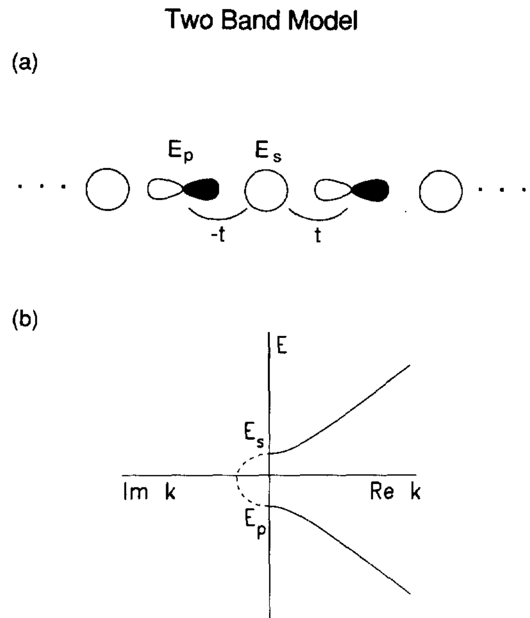

FIG. 1 (a) Schematic of the orbitals used to generate our two-band model. (b) Complex band structure for the two band model.

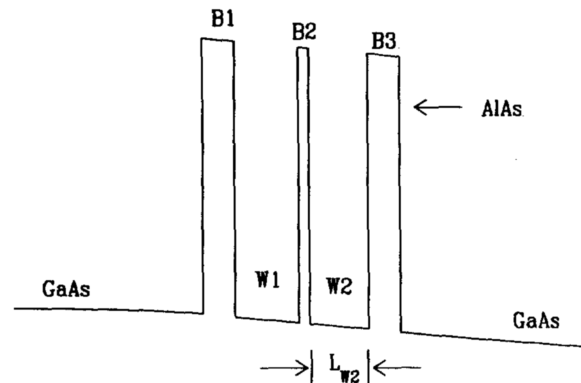

FIG. 2. Illustration of a GaAs/AlAs asymmetric triple-barrier heterostructure. Note that the widths of well 1 (L_{W1}) and well 2 (L_{W1}) can be different.

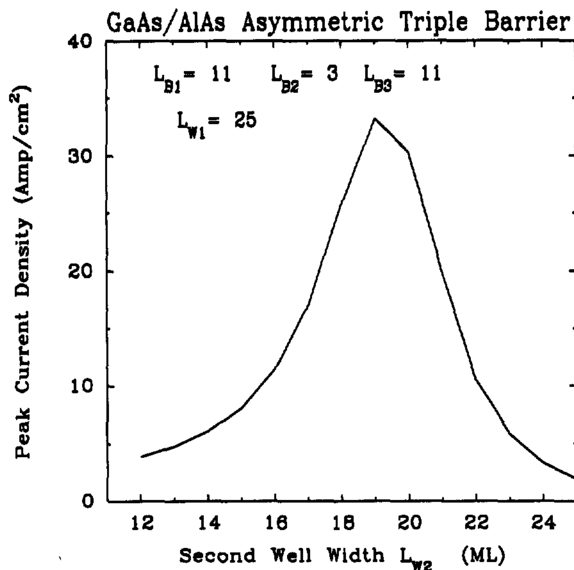

FIG. 3. Theoretical peak current density at the first resonance peak for a series of GaAs/AlAs asymmetric triple barrier devices in which the width of the second well is varied.

Previous studies have shown that symmetric triple barrier structures ($L_{W1} = L_{W2}$) can exhibit interesting electrical properties, including high peak-to-valley current ratios.[13] For the symmetric device, under flat band conditions the lowest two quasibound states are symmetric and antisymmetric with respect to the center of the device. This, of course, is the result of mixing of the states in the two quantum wells. Under positive applied bias, however, the bottom of W2 is lowered with respect to the bottom of W1, resulting in increased separation of the energy levels of the lowest two quasibound states. Consequently, the mixing quickly disappears as applied bias increases, leaving the lowest and second lowest quasibound states localized separately in W2 and W1, respectively. In fact, for the symmetric device we examined,[13] the first (second) peak in the I–V curve results from resonant tunneling through the quasibound state strongly localized in W2 (W1).

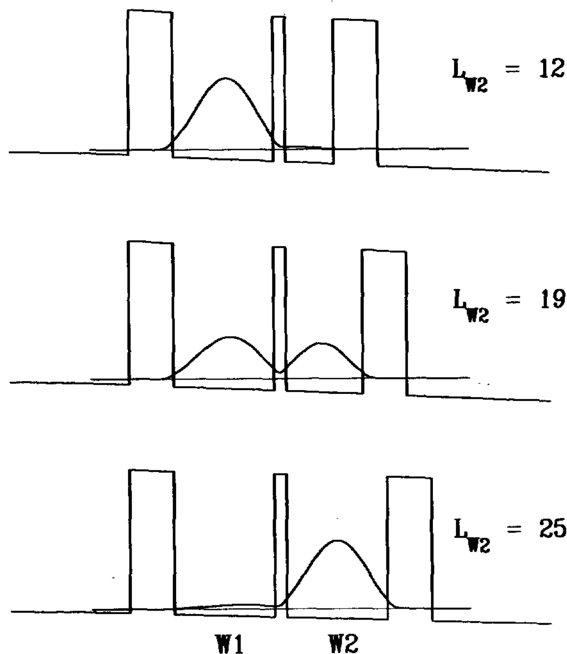

FIG. 4. Probability densities of the lowest quasibound states for three GaAs/AlAs asymmetric triple barrier devices under applied bias. The applied bias for each device is the voltage at which the lowest peak in current occurs. In all cases, $L_{W1} = 25$.

Mixing can be reintroduced for biased devices if we consider the asymmetric triple barrier structures where L_{W1} and L_{W2} can be different. For a fixed L_{W1}, we can find the appropriate L_{W2} for which mixing of the quasibound states in W1 and W2 occurs.

In our study, we examine a series of triple barrier structures with fixed barrier widths ($L_{B1} = 11$, $L_{B2} = 3$, $L_{B3} = 11$, in monolayers). L_{W1} is fixed at 25 monolayers while L_{W2} varies from 12 to 25 monolayers. For each device in the series, we compute a J–V curve, and note how the positions and peak current densities change with the width of W2. This allows us to study the dependence of the device J–V characteristics on the nature of the quasibound state wave function in a controlled manner.

In Fig. 3, we present the theoretical peak current density of the first resonance peak as a function of L_{W2}. Over the range shown, the peak current density is found to vary considerably, with the maximum peak current density (for $L_{W2} = 19$) being an order of magnitude higher than those found in the narrow well ($L_{W2} = 12$) and symmetric triple barrier ($L_{W2} = 25$) cases.

This can be understood if we examine the nature of the quasibound states through which resonant tunneling occurs. In Fig. 4 we plot the probability densities of the lowest quasibound states for the three cases mentioned above (i.e., $L_{W2} = 12, L_{W2} = 19$, and $L_{W2} = 25$). In each case, the bias applied to the device is the voltage at which the first current peak occurs. We see that for the symmetric ($L_{W2} = 25$) case, the probability density is mainly localized in W2. Consequently, while the quasibound state interacts relatively strongly with the continuum states in the right electrode, the interaction with the continuum states on the left electrode is weak. A similar argument can be made for the $L_{W2} = 12$ case. In the $L_{W2} = 19$ case, however, the quasibound state wave function is spread out over both wells, and interacts strongly with the continuum states in both electrodes. This makes it a better "tunneling channel" between the two electrodes than the quasibound states in the $L_{W2} = 12$ and $L_{W2} = 25$ cases, and hence the peak current density is the highest in this device.

In Fig. 5, the calculated peak positions of the lowest two resonance peaks in the J–V curves are plotted as functions of L_{W2}. For small L_{W2}, the lower and upper branches correspond to tunneling through quasibound states localized in the first and second well, respectively. For large L_{W2}, the situation is reversed. In the intermediate range, as we have

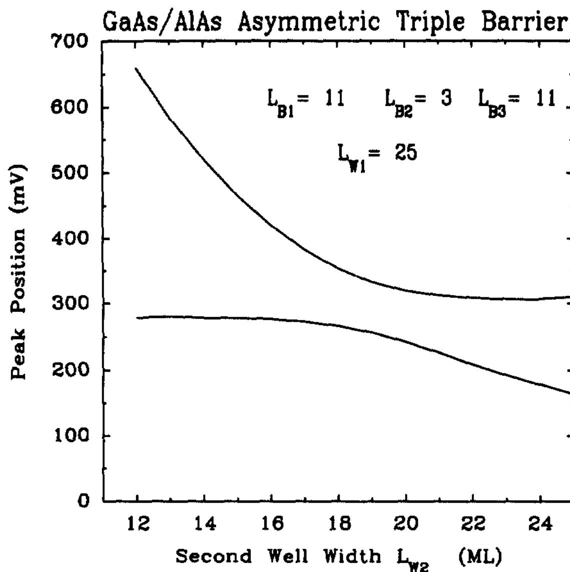

FIG. 5. Applied biases at which the lowest two resonance peaks for the GaAs/AlAs asymmetric triple barrier devices occur. Note the characteristic anticrossing behavior of the two levels.

seen earlier, tunneling occurs via states which are extended across both the first and the second well, and a clear anticrossing behavior between the two branches is seen. This behavior is an indication of the coherence of the quasibound states in the two quantum wells.

B. Broken-gap resonant interband tunnel devices

In this section we model the InAs–GaSb–InAs interband tunnel device. A band diagram of this device is shown in Fig. 6. Note that the energy gaps of the two materials do not overlap, so there is a broken-gap energy range between the InAs conduction band edge and the GaSb valence band edge. This allows electrons in InAs with energies in the broken-gap energy range to tunnel through the GaSb layer via the GaSb valence band states, as indicated by the dash-dot line in Fig. 6.

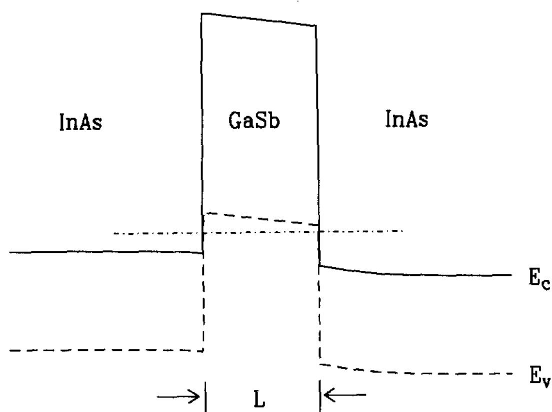

FIG. 6. Band diagram of an InAs–GaSb–InAs broken-gap interband tunnel device. Note that an electron can tunnel through the GaSb layer via the GaSb valence bands, as indicated by the dot–dash line.

In Fig. 7(a) we show the transmission coefficient over the broken-gap energy range for the InAs–GaSb–InAs structure under flatband conditions. The transmission curve exhibits the familiar Lorentzian shape, indicating the presence of a quasibound state. The nature of this quasibound state, however, is quite different from the quasibound states found in conventional double barrier type structures. In the double-barrier structure, the quasibound states are associated with the presence of classically forbidden barrier regions. In the InAs–GaSb–InAs structure, the quasibound states result from the imperfect coupling of wave functions at the InAs/GaSb interfaces. Comparing the transmission resonance of the InAs–GaSb–InAs structure to that for a InAs/AlSb double barrier structure, shown in Fig. 7(b), we find that the resonance width is considerably wider than in the double barrier structure, even for barrier width of only 3 monolayers. This is because tunneling via a quasibound state in the InAs–GaSb–InAs structure does not involve traversing classically forbidden regions as is required in the double barrier structures. The fact that resonant tunneling can occur without the presence of classically forbidden barrier regions can have important practical consequences. The characteristic wide transmission resonances can result in (1) NDR with high peak current densities and (2) short tunneling times, which are crucial for high speed applications.

We have grown and characterized three InAs–GaSb–InAs structures with GaSb layer thicknesses of 20, 50 and

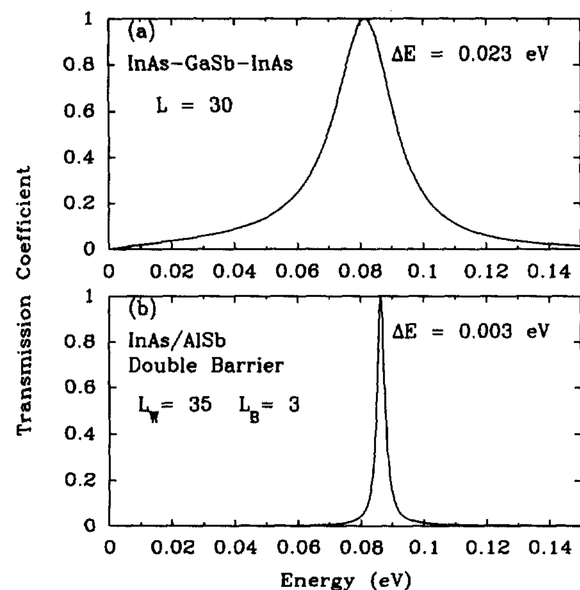

FIG. 7. Transmission coefficient for (a) an InAs–GaSb–InAs broken-gap interband tunnel device, and (b) an InAs/AlSb double barrier heterostructure with thin barriers. Note that the resonance is much narrower for the InAs–GaSb–InAs, despite the thin barriers in the InAs/AlSb double barrier structure.

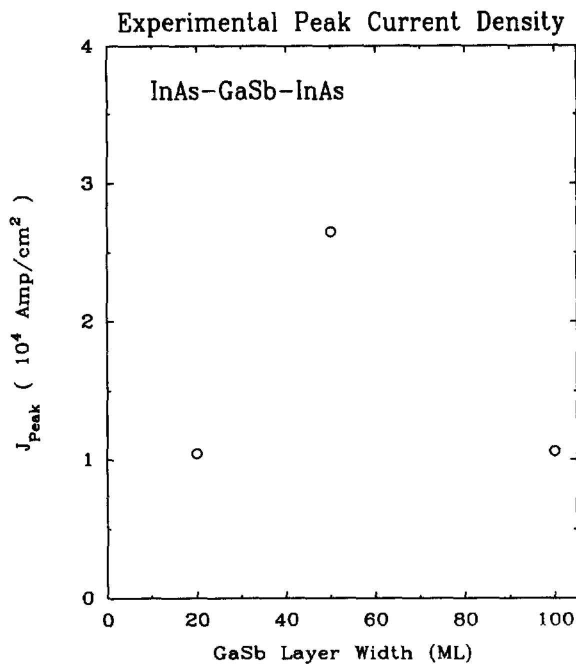

FIG. 8. Experimental peak current densities for InAs–GaSb–InAs broken-gap interband tunnel devices with GaSb layer width of 20, 50, and 100 monolayers.

100 monolayers. Figure 8 shows the measured peak current density at resonance for these three structures. The 20 and 100 monolayer samples show peak current densities of 1×10^4 A/cm^2, while the sample with the intermediate well width (50 monolayers) has the largest peak current density. It was also observed that while the 50 and 100 monolayer samples showed NDR with peak-to-valley current ratios of 1.6–2.0, the 20 monolayer sample showed a very small P/V ratio of ≈ 1.1.

In Fig. 9 we show theoretical peak current densities as a function of GaSb layer thickness. Resonance peaks were not seen in the calculated J–V curves for GaSb layer thicknesses below 20 monolayers. Above 20 monolayers, as the GaSb layer thickness increases, the peak current density increases until reaching a maximum at 30 ML, and then decreases in general but with occasional secondary maxima.

We can understand this behavior by examining a catalog of the transmission resonances in the broken-gap region. In Fig. 10 the widths of the transmission resonances are plotted as functions of GaSb layer thickness. Different resonances in the same structure are shown with different symbols. As the GaSb layer thickness increases, more transmission resonances appear in the broken-gap region, but the resonance widths in general decrease with increasing GaSb layer thickness. Since wide resonances contribute more to the current density, this explains the general trend of decreasing peak current density with increasing GaSb layer thickness. The secondary maxima can be explained by the appearance of additional transmission resonances as the GaSb layer thickness is increased.

Figure 11 shows the transmission coefficients in the broken-gap energy range for three representative cases ($L = 15$, 30, 100 monolayers) of the InAs–GaSb–InAs structures under flatband conditions. The corresponding calculated J–V curves are shown in Fig. 12. When the GaSb layer is very narrow ($L = 15$), there are no quasibound states in the broken-gap, and therefore no transmission re-

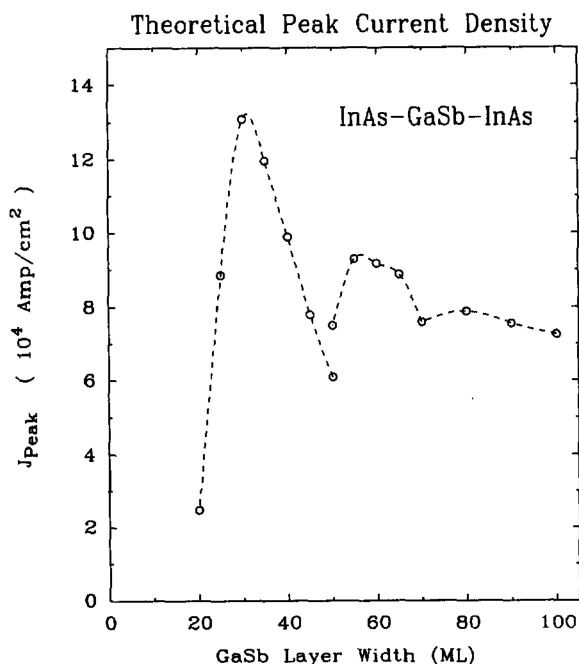

FIG. 9. Theoretical peak current density for the InAs–GaSb–InAs broken-gap interband tunnel device as a function of GaSb layer width.

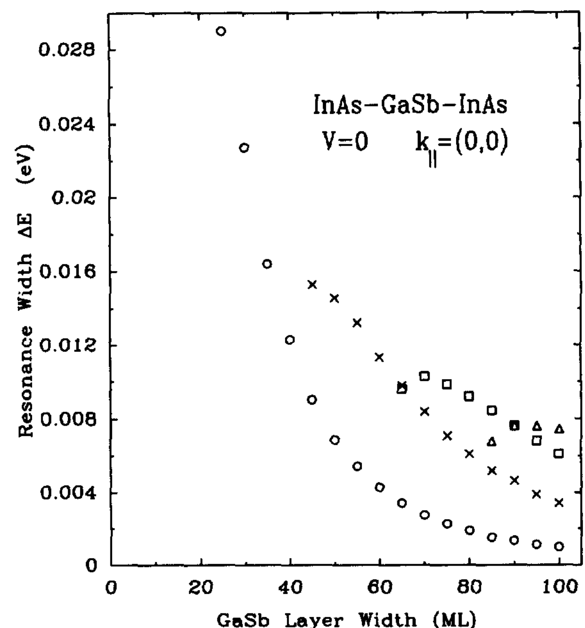

FIG. 10. Transmission resonance widths for the InAs–GaSb–InAs interband tunnel device as functions of GaSb layer width. First, second, third, and fourth peaks are marked with ○, ×, □, and △, respectively.

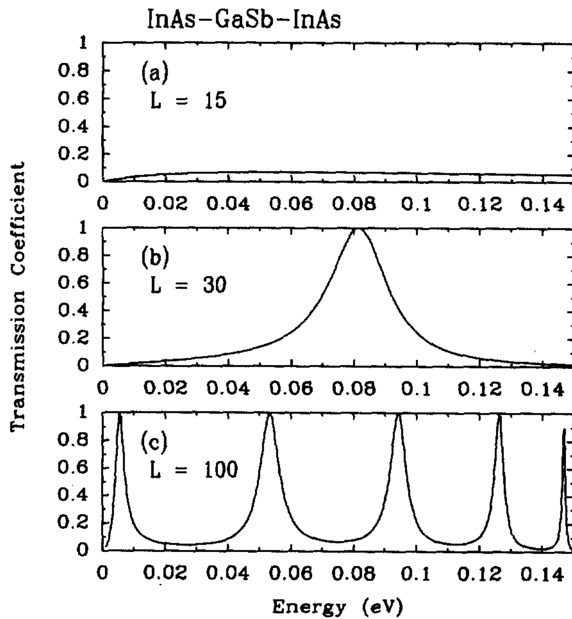

FIG. 11. Flatband transmission coefficient in the broken-gap energy range for InAs–GaSb–InAs interband tunnel devices with GaSb layer widths of 15, 30, and 100 monolayers.

sonances are observed. Note that since there are no classically forbidden regions for electrons in this energy range, the transmission coefficient is still quite large (a few percent) even in the absence of any resonances. The J–V curve for this device shows no clearly identifiable current peaks; the current is associated with nonresonant tunneling. The $L = 30$ device has the highest calculated peak current density. The

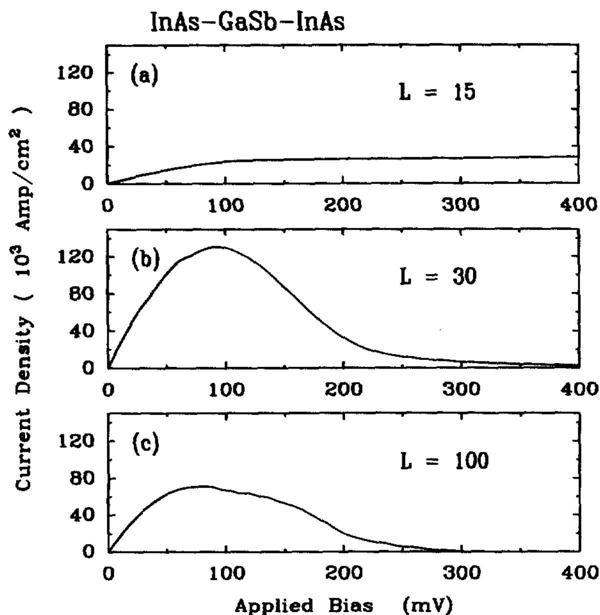

FIG. 12. Theoretical J–V curves for InAs–GaSb–InAs interband tunnel device of GaSb layer widths of 15, 30, and 100 monolayers.

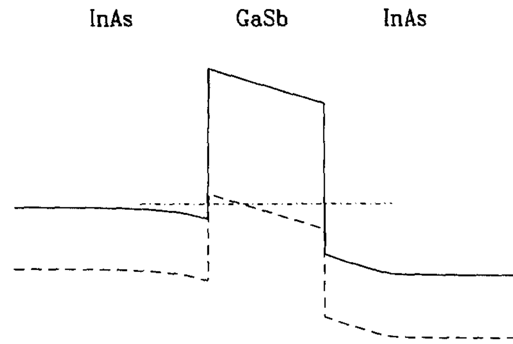

FIG. 13. Shutoff mechanism in InAs–GaSb–InAs tunnel device. At high bias, electrons need to tunnel through the GaSb gap region, greatly reducing the tunneling probability.

calculated J–V curve clearly shows NDR, and the transmission coefficient contains a single wide resonance in the broken-gap energy range. The transmission coefficient for the $L = 100$ structure shows several relatively narrow resonances; the J–V curves shows NDR, but has a smaller peak current density than the $L = 30$ structure.

Our theoretical analysis is in good general agreement with the observed experimental trends, namely: (1) Peak current density is low for the narrow GaSb layer, rises to a maximum and then follow a general decreasing trend. (2) NDR is less pronounced in the sample with narrow ($L = 20$) GaSb layer. Furthermore, our analysis indicates that a resonant tunneling process is involved in the devices where NDR is observed.

In a recently reported result Taira *et al.*[7] attributed the observed NDR in a $L = 100$ InAs–GaSb–InAs structure to Ohmic conduction of electrons through the GaSb valence bands which eventually was shut off when the applied bias became high enough that the electrons had to tunnel through the GaSb gap region. (See Fig. 13.) Taira *et al.*, however, questioned this explanation since the attributed mechanism should produce a much more gradual drop in the current than was observed in the NDR region. While the shutoff mechanism pictured in Fig. 13 is certainly important, our data and analysis indicate that quantum effects play a nontrivial role in the operation of the device. If Ohmic conduction and the shutoff mechanism were solely responsible for the observed NDR, then the variation in peak current density with GaSb layer width should be monotonic. Our theoretical prediction and experimental observations that the peak current density and the peak-to-valley current ratio are lower in the 20 monolayer barrier sample than the 50 monolayer barrier sample, indicate that a resonant tunneling process is pivotal in producing the observed NDR in these devices.

IV. SUMMARY AND CONCLUSIONS

We have developed a computationally efficient method for computing current–voltage characteristics of conven-

tional as well as interband tunnel devices based on a simple two-band model.

Using this method, we have examined GaAs/AlAs asymmetric triple barrier structures. We found that by engineering the nature of the quasibound state wave functions, we could dramatically influence the *J–V* characteristics of the device. In particular, higher peak currents should be found in devices designed to have quasibound states with wave functions which interact more strongly with continuum states in both the right and left electrodes. In addition, we found that the coherence between quasibound states in the two quantum wells should be observable in the current–voltage characteristics of the devices.

We have also examined the InAs–GaSb–InAs broken-gap interband tunnel device; this structure is distinguished by the absence of classically forbidden barrier regions, leading to very wide transmission resonances. Our data and analysis indicate that a resonant tunneling process plays a pivotal role in producing the observed NDR. Furthermore, we have found that highest peak current densities should be found in devices with GaSb layer thicknesses corresponding to a singe rather than multiple transmission resonance peaks in the broken-gap region.

ACKNOWLEDGMENTS

The authors would like to thank Y. C. Chang, J. R. Söderström, M. K. Jackson, and Y. Rajakarunanayake for helpful discussions. This work is supported by the Office of Naval Research (ONR) under Grant No. N00014-89-J-1141.

[1]R. Tsu and L. Esaki, Appl. Phys. Lett. **22**, 562 (1973).

[2]L. L. Chang, L. Esaki, and R. Tsu, Appl. Phys. Lett. **24**, 593 (1974).

[3]M. Sweeny and J. Xu, Appl. Phys. Lett. **54**, 546 (1989).

[4]J. R. Söderström, D. H. Chow, and T. C. McGill, Appl. Phys. Lett. **55**, 1094 (1989).

[5]L. F. Luo, R. Beresford, and W. I. Wang, Appl. Phys.Lett. **55**, 2023 (1989).

[6]D. H. Chow, J. R. Söderström, E. T. Yu, and T. C. McGill (to be published).

[7]K. Taira, I. Hase, and K. Kawai, Proceedings of the Seventh International Workshop on Future Electron Devices, Superlattice and Quantum Functional Devices, Oct. 2–4, 1989, Toba, Japan (unpublished), pp. 191, 192.

[8]D. A. Collins, D. H. Chow, and T. C. McGill (to be published).

[9]See, for example, J. N. Schulman and Y. C. Chang, Phys. Rev. B **27**, 2346 (1983).

[10]J. R. Söderström, E. T. Yu, M. K. Jackson, Y. Rajakarunanayake, and T. C. McGill (to be published).

[11]See, for example, J. N. Schulman and Y. C. Chang, Phys. Rev. B **24**, 4445 (1981).

[12]C. B. Duke, *Solid State Physics, Suppl. 10, Tunneling in Solids* (Academic, New York, (1969).

[13]D. A. Collins, D. H. Chow, D. Z.-Y. Ting, E. T. Yu, J. R. Söderström, and T. C. McGill, *Proceedings of the Sixth International Conference on Hot Carriers in Semiconductors* [Solid-State Electronics **32**, 1095 (1989)].